Materials Research
Express

High-temperature and melting behaviour of nanocrystalline refractory compounds: an experimental approach applied to thorium dioxide

F Cappia[1,2], D Hudry[1], E Courtois[3], A Janßen[1], L Luzzi[2], R J M Konings[1] and D Manara[1]

[1] European Commission, Institute for Transuranium Elements, PO Box 2340, 76125 Karlsruhe, Germany
[2] Politecnico di Milano, Department of Energy, 'Enrico Fermi' Center for Nuclear Studies, via Ponzio, 34/3—20133 Milan, Italy
[3] Karlsruhe Institute of Technology, Institute for Nanotechnology, 76344 Eggenstein-Leopoldshafen, Germany
E-mail: Fabiola.CAPPIA@ec.europa.eu and Dario.MANARA@ec.europa.eu

Received 21 March 2014
Accepted for publication 29 April 2014
Published 4 June 2014
Materials Research Express **1** (2014) 025034
doi:10.1088/2053-1591/1/2/025034

Abstract

The behaviour from 1500 K up to melting of nanocrystalline (nc) thorium dioxide, the refractory binary oxide with the highest melting point (3651 K), was explored here for the first time using fast laser heating, multi-wavelength pyrometry and Raman spectroscopy for the analysis of samples quenched to room temperature. Nc-ThO_2 was melted at temperatures hundreds of K below the melting temperature assessed for bulk thorium dioxide. A particular behaviour has been observed in the formed liquid and its co-existence with a partially restructured solid, possibly due to the metastable nature of the liquid itself. Raman spectroscopy was used to characterize the thermal-induced structural evolution of nc-ThO_2. Assessment of a semi-empirical relation between the Raman active T_{2g} mode peak characteristics (peak width and frequency) and crystallites size provided a powerful, fast and non-destructive tool to determine local crystallites growth within the nc-ThO_2 samples before and after melting. This semi-quantitative analysis, partly based on a phonon-confinement model, constitutes an advantageous, more flexible, complementary approach to electron microscopy and powder x-ray diffraction (PXRD) for the crystallite size determination. The adopted experimental approach (laser heating coupled with

Raman spectroscopy) is therefore proven to be a promising methodology for the high temperature investigation of nanostructured refractory oxides.

S Online supplementary data available from stacks.iop.org/MRX/1/025034/mmedia

Keywords: nanocrystalline thorium dioxide, melting point depression, fast laser heating, micro-Raman spectroscopy

1. Introduction

The last two decades have witnessed a growing interest toward the synthesis of nanocrystals (NCs) within a broad range of chemical compositions [1, 2]. NCs constitute interesting building blocks of both fundamental and technological importance because of their size-and shape-dependent properties [3–6]. Hence, determining the modification of physical and chemical properties of nanomaterials as a function of size and shape is of prime importance in order to design novel nanomaterials with innovative functional properties. Such a goal constitutes a particularly challenging task when dealing with very high temperatures. The use of refractory nanomaterials conceived to operate under extreme conditions, could be limited because of the melting point variation. Melting point depression of free NCs was indeed theoretically predicted since 1871 [7] and 1909 [8], based on the higher contribution to the solid′s free energy due to the large surface/interface area, compared with bulk materials. Much more recently, this effect was experimentally observed for low-dimensional metals and semiconductors [9–15]. Due to the extreme conditions (temperatures above 2500 K, high vapour pressure, reactivity with the containment etc), neither nanocalorimetry, high-temperature x-ray diffraction, *in situ* electron microscopy nor other thermal analysis techniques usually employed to study nanomaterials [9–15] can be applied to refractory nanomaterials.

In this paper, laser heating under self-container conditions and controlled atmosphere [16] was applied to nc-ThO_2 up to high temperature, well beyond 3000 K. The sample radiance temperature was recorded by fast multi-wavelength pyrometry, while a laser-probe signal was used to detect the eventual formation of liquid on the sample surface. The sample's crystalline structure as well as crystallite size and morphology were analysed before and after laser heating cycles by means of scanning and transmission electron microscopy (SEM, TEM), powder x-ray diffraction (PXRD) and micro-Raman spectroscopy (μRS). Although the latter is an analytical method widely applied to nanomaterials [17–26], it is employed here in a peculiar fashion. The characteristic broadening of vibrational peaks, related to the confinement of phonons in crystallites whose dimensions are small (indicatively below 50 nm) [17], is directly correlated to the crystal grain size in order to obtain a semi-empirical relation. Such a relation is then used to estimate the local grain size after the laser heating experiments. This approach complements therefore TEM and PXRD characterizations. It is even in a way more flexible, in that it permits a local analysis of the sample surface which can be only partially melted or agglomerated following the laser heating. For example, if a sub-second thermal excursion over 3000 K induced by laser-heating in a nano-structured solid leads to the formation of microscopic crystallites on extended areas, this can be taken as a clear sign that part of the material

underwent a melting/freezing transition. The sub-second, local formation of such macroscopic crystallites can be easily observed with the help of the current Raman spectroscopy approach.

Thorium dioxide has the highest melting point among the common oxides (3651 K [27]), good chemical stability toward oxygen [28] and good sensitivity to Raman scattering [29]. It has therefore been chosen as a test material to initiate this kind of experimental study. The current results provide a first insight on the high-temperature stability of this newly synthesised material [30, 31].

Finally, it should be added that investigations on the thermal stability of actinide-based nano-oxides are of particular interest both to deepen thermodynamic properties of actinides and to explore their potential applications in the nuclear industry [32], e.g. as advanced fuels [33].

2. Materials and methods

2.1. nc-ThO_2 preparation

ThO_2 NCs were synthesized by a non-aqueous method described elsewhere [30, 31]. The as-prepared NCs were used to prepare nc-ThO_2. Dried ThO_2 NCs were compacted with a hydraulic press ($P \approx 3$ MPa). Then, the resulting pellets (3 mm in diameter and a few mm of thickness, depending on the amount of material available, typically between 10 mg and 50 mg) were heat treated under air for 1 h at 600 K and 700 K in order to remove organic ligands used to stabilize the ThO_2 NCs [30, 31]. The preliminary heat treatment was necessary in order to avoid the fast vaporization of the organic ligands during laser heating, resulting in the loss of the mechanical integrity of the pellet. The heat treatment did not produce any excessive crystallite growth whose size was (4 ± 1) nm, as estimated from TEM images and Rietveld refinement of PXRD patterns. Furthermore, Raman spectra recorded on the annealed powder revealed that ligand removal was nearly complete, as the peaks characteristic of the ligand mostly disappeared.

2.2. Laser heating technique and experimental procedure

Bulk-refractory oxides have been successfully melted using sub-second laser heating coupled with pyrometry. A full description of the experimental apparatus employed in this study and related background can be found elsewhere [16, 34–37]. The tuneable fast heating typical for this experimental approach (power versus time profile is programmable with a resolution of 1 ms) is crucial in order to limit grain agglomeration and growth and study the high-temperature behaviour of nanomaterials, including a possible melting point variation as a function of the crystallite size. The sample, held in an autoclave under controlled atmosphere (dry air pressurised at 0.3 MPa), is heated by a 4.5 kW cw Nd:YAG TRUMPF® laser. The nc-pellet was held in a crucible made of bulk-ThO_2. Bulk-ThO_2 was used in order to avoid crucible melting and chemical reactions with the sample itself. Upon the heating stage, possible phase changes and, in particular, the eventual onset of melting is detected by the appearance of vibrations in the signal of an Ar^+ probe laser reflected by the sample surface (Reflected Light Signal technique, or RLS) [16]. The sample cools naturally when the laser beam is switched off. The sample surface temperature is recorded by fast pyrometers on a circular spot of half a millimetre in radius. These pyrometers operate in the visible-near infrared range between 550 nm and 920 nm, and are calibrated against a tubular graphite blackbody cavity. The reference pyrometer

wavelength is here 655 nm, directly calibrated with a standard W-filament lamp according to the procedure reported in [16].

The normal spectral emissivity (ε_λ) of bulk- and nc-ThO_2 was measured by fitting the radiance spectra recorded by 180 photo-detectors between 550 nm and 920 nm. This parameter was then used to obtain the sample surface temperature from the radiance intensity L_λ measured by the reference pyrometer at 655 nm, by using Planck′s equation for a real surface [16]:

$$L_\lambda(T) = \frac{c_{1L}}{n^2 \cdot \lambda^5} \cdot \varepsilon_\lambda \cdot \left[\exp\left(\frac{c_2}{n \cdot \lambda \cdot T} \right) - 1 \right]^{-1} \quad (1)$$

where λ is the wavelength, T the absolute temperature, $c_{1L} = 2\,h \cdot c_0^2$ is the first radiation constant and $c_2 = h \cdot c_0 \cdot k_B$ is the second radiation constant, where c_0 is the speed of light in vacuum, h Planck's constant, and k_B Boltzmann's constant. For the purposes of the present work, the index of refraction is always taken to be equal to 1 (being the current medium air or an inert gas close to atmospheric pressure). Most refractory oxides, like ThO_2, display few or no electronic transitions in the visible-near infrared spectral range explored in this research. It is therefore reasonable to apply in in this spectral domain the simplifying hypothesis that ε_λ is independent of the wavelength (grey body assumption).

Various experimental techniques were used to characterize the sample before and after the laser heating cycle, i.e. PXRD, SEM, EDX, TEM and micro-Raman spectroscopy. Synthetic schemes of the entire experimental procedure as well as the laser heating system and details about the experimental characterization techniques employed can be found in the online supplementary data (stacks.iop.org/MRX/1/025034/mmedia).

3. Results and discussion

3.1. Raman spectroscopy: calibration curve

Red shift and broadening of the triply degenerate T_{2g} peak of ThO_2 fluorite structure in nanocrystalline samples has already been observed in previous research [38, 39]. In this study, small (microgram) nanocrystalline samples were annealed under air in a furnace at different temperatures to induce particle growth and to track the evolution of the peak characteristics with the mean grain size.

Bulk ThO_2 was used as a reference. The T_{2g} peak was measured at 465 cm^{-1} [29, 40] with a full width at half maximum (FWHM) of 7.73 cm^{-1}. Interestingly, figure 1(a) shows a progressive red shift and broadening of the T_{2g} peak when the crystallite size gets smaller. In particular, the effect is more pronounced at very small dimensions. Size of the evolved crystallites was determined using TEM image analyses, and, in one case, it was also possible to confirm results from Rietveld refinement of PXRD pattern, as reported in table S1 and figures S1 and S2 in the online supplementary data.

Several factors can contribute to the observed changes in the Raman peak position and linewidth. These include phonon confinement, strain, broadening associated with the size distribution, defects, and variations in phonon relaxation with particle size [20]. In particular, phonon confinement leads to the relaxation of the $q \approx 0$ selection rule for finite-size crystals [17, 41, 42]. The phonon confinement model has been applied to compare experimental data with theoretical predictions in the nanostructured samples (see appendix A). Further studies are needed to fully develop this aspect of the research.

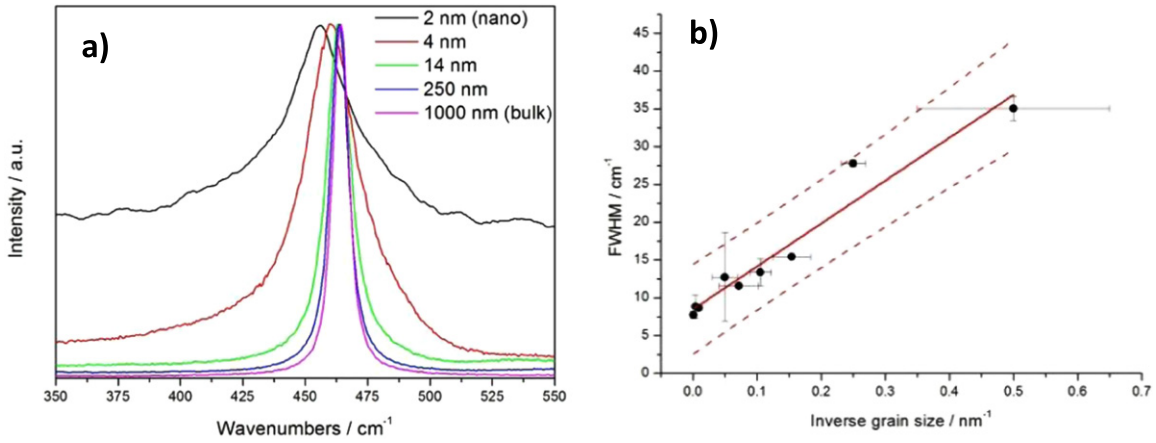

Figure 1. (a) Magnification of the T_{2g} peak of nc-ThO_2 samples with different crystallite size and of bulk-ThO_2. Excitation laser wavelength: 488 nm. Only the peaks of most significant samples are shown. (b) FWHM versus inverse of grain size[4]. Dashed lines represent ±95% confidence bands in the linear regression fit. When the grain size approaches infinity (like in the bulk material) uncertainty bands lose their physical meaning.

At this stage and for the aim of the present study, peak characteristics (i.e. peak position and FWHM) were empirically used as a fingerprint of the local crystallite size. The FWHM was less affected than the peak position by laser parameters that cannot be precisely controlled (i.e., polarization, laser power). Therefore, the FWHM was chosen as the most reliable parameter to be correlated to the inverse grain size, as reported in figure 1(b). Despite some scattering most probably related to inhomogeneity in the particle size after the annealing, the grain size dependence of the Raman T_{2g} peak half-width can be fitted reasonably well with a linear interpolation, as already reported for other nanocrystalline materials [26].

3.2. Laser heating and application of micro-Raman spectroscopy

Figure 2(d) reports the thermogram obtained from a laser heating experiment performed on an nc-ThO_2 sample whose average crystallite size is 4 nm. Additionally, a reference thermogram obtained for bulk ThO_2 (average crystallite size of 1 μm), and recorded with the same experimental conditions is added for comparison in figure 2(a).

The thermogram of bulk ThO_2 (figure 2(a)) shows delay in temperature rise, due to semitransparency to the laser wavelength [27]. This corresponds to an anomalous increase observed in the optical absorptivity/emissivity of thoria at temperatures between 1500 K and 2000 K. It has been attributed [27] to absence of 5f electrons in thorium, shifting, at room temperature, the optical absorption band to energies beyond the visible range. At higher temperature, instead, visible light absorption is permitted by a considerable increase of the oxygen defect concentration. Interestingly, such a phenomenon is much less pronounced in the nc-ThO_2 curve (figure 2(d)), possibly related, in the nanomaterial, to effects of the large grain boundary area on the actual oxygen defect concentration, even at room temperature.

The literature high-temperature spectral emissivity value for bulk thorium dioxide is $\varepsilon_\lambda = 0.87$ [27], experimentally confirmed and adopted here also. On the other hand, it is well known that the emissivity of small particles can vary with their radius, as a direct consequence

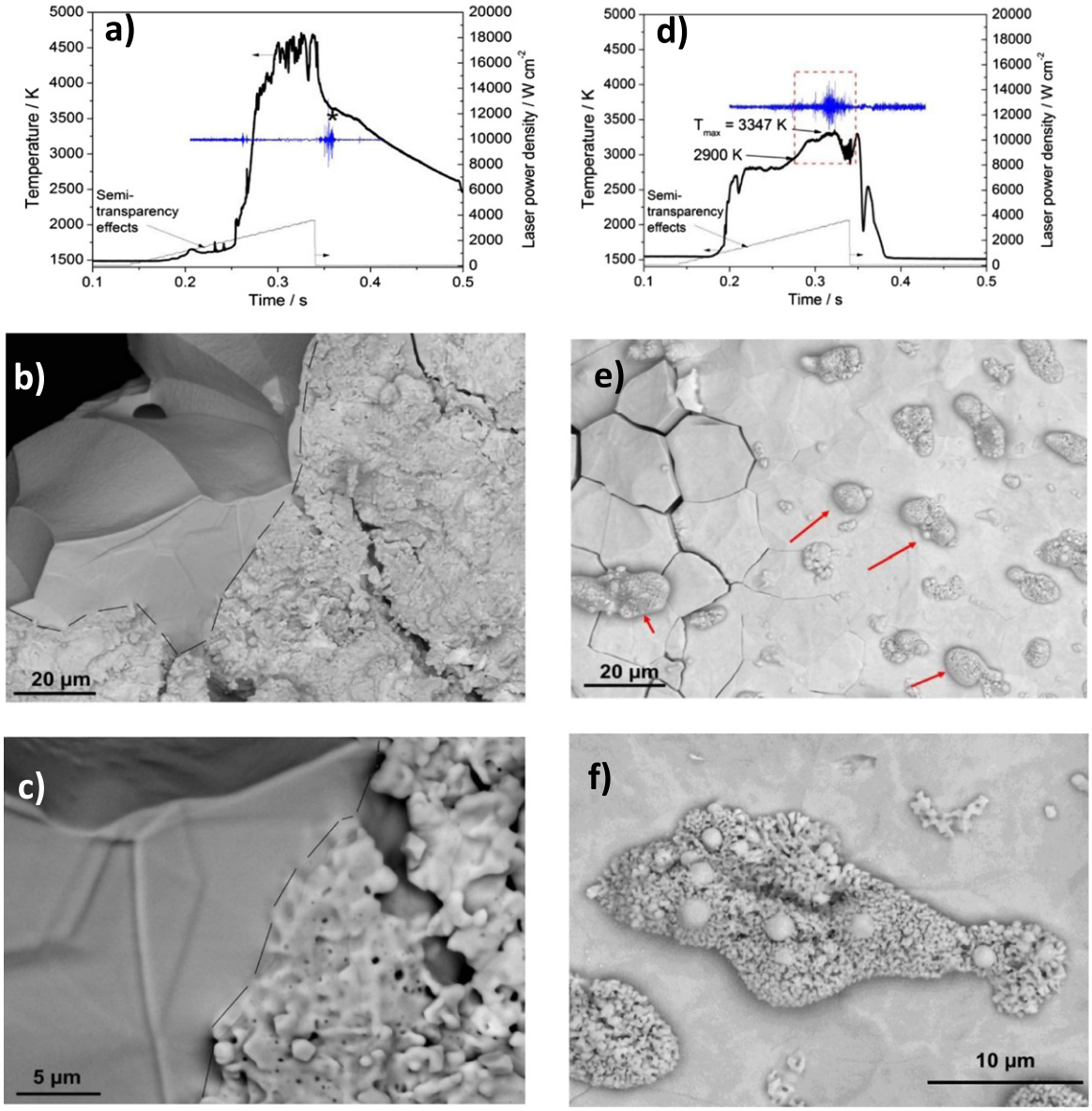

Figure 2. (a) Thermogram of bulk ThO_2. The blue solid line shows RLS from sample surface[4] and indicates the solidification temperature recorded for bulk ThO_2 after switching off the laser (3631 K). (b), (c) BSE images of the molten bulk ThO_2 sample. In both images the interface between molten (left part) and unmolten (right part) zones, highlighted by a dashed black line, is clearly visible. (d) Thermogram of the nc-ThO_2. Blue solid line shows RLS from sample surface. Dashed red square shows vibrations on the RLS signal which can be attributed to the formation of liquid on the nc-ThO_2 sample surface. (e) BSE image of the laser-heated nc-ThO_2 sample. Red arrows indicate aerosols re-deposited on sample surface. The base layer is homogeneous and characterized by several cracks, due to the high temperature gradients during heating/cooling process. The almost complete absence of porosity is remarkable here, very similar to the molten mass in bulk ThO_2. (f) BSE image of aerosol particles re-deposited on the sample surface upon cooling.

of the geometrical absorption cross section dependence on the particle size [43]. In the present investigation, the emissivity of nc-ThO_2 was measured using the mentioned multi-wavelength pyrometry approach with the above-mentioned grey-body assumption. In the wavelength range of operation, the measured mean value of emissivity was 0.74. This value was therefore adopted in order to obtain the real sample temperature from the radiance emitted by the hot bulk-or nc-ThO_2 sample through equation (1) [16].

The temperature reached in the bulk ThO_2 sample was well beyond the melting temperature of the bulk material (here detected at 3631 K, in good agreement with literature [27]), whereas the temperature in nc-ThO_2, heated with the same laser power profile, never exceeded 3350 K. In the latter case, the RLS curve revealed, in the temperature range 2900–3300 K, the onset of vibrations which might correspond to the presence of liquid formed from nano-structured ThO_2 at temperatures considerably lower than the melting point of bulk ThO_2.

The radiance signal (thermogram in figure 2(d)) recorded on the nano-structured sample lost stability at temperatures much lower than the one corresponding to the bulk sample: after a steep increase, the temperature oscillates broadly without any further increase. This feature can be partly due to non-congruent evaporation/mechanical instability of the surface under the laser beam, but it can also be a consequence of the metastability of the liquid probably formed with respect to resolidification into bulk solid [44, 45]. Small systems can exhibit phase changes different from those of bulk matter, with dynamical coexistence of phases in a more or less extended temperature range [45]. Statistical thermodynamic theory of small systems has been extended to explain formation and persistence of such metastable states [44, 46]. The fact that the shape of the thermogram could be affected by the metastability of the forming liquid is still an intriguing open question to be deepened in further research. Independently, proving that melting was actually produced in nc-ThO_2 at a temperature considerably lower than that foreseen for the bulk material, constitutes a somewhat difficult challenge. Comparing the microstructures of the bulk- and nc-ThO_2 can shed some light on this question. The microstructures of bulk- and nc-ThO_2 after laser heating are shown in figure 2(b), (c), (e), (f), respectively. Figure 2(b) and (c) show the interface between the molten pool (left part) and unmolten zone (right part) of the bulk ThO_2 sample. Some differences between the microscopic structure of the unmolten and molten bulk ThO_2 are clearly visible. The molten part displays a dense, homogeneous structure free of porosity, features typical for recrystallization from a liquid [47]. Instead, the unmolten part is characterized by partially sintered grains whose size is below 5 μm and characteristic high residual porosity [48]. Post-melting SEM images of the nc-ThO_2[5] sample (figure 2(e)) showed a homogeneous base layer displaying several similarities with the molten zone of the bulk sample. Thus, the formation of such microscopic crystallites as a result of a sub-second heating would certainly be attributable to melting and resolidification rather than mere grain agglomeration. Partial vaporisation of the ThO_2 nano-crystallites certainly occurred, too, as signified by the presence of 'aerosol' spots on the sample surface

[4] Particles were assumed to be spherical, based on phonon confinement model [42]. This was reasonable for heat-treated particles, but not for as-synthesised samples, which were composed of nanorods. The spectra recorded are the result of average confinement of phonons in both dimensions. The diameter of 'equivalent' sphere of same volume as the rod was assumed as characteristic dimension for comparison with the other samples.

[5] It is not strictly correct to speak about nanostructured material after melting experiments. However, the name is here used to clearly distinguish the original nc-ThO_2 sample from the bulk one.

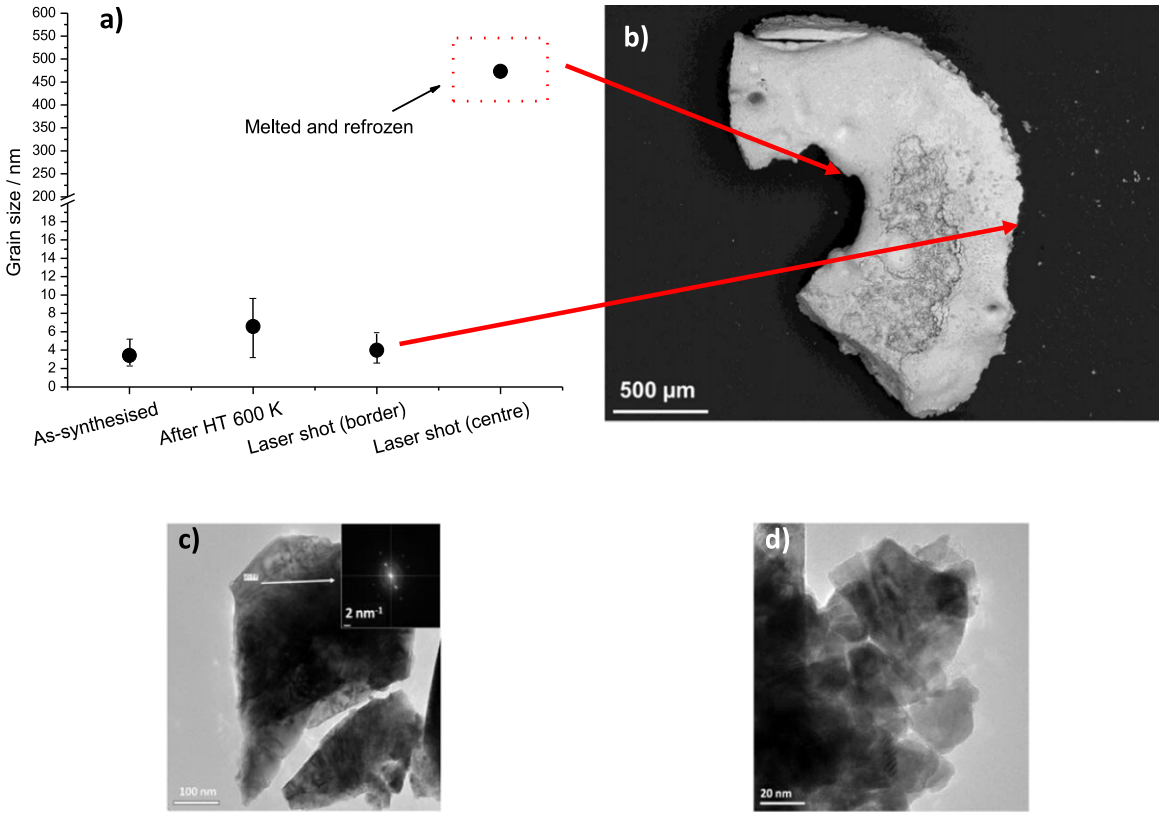

Figure 3. (a), (b) Application of Raman spectroscopy to determine grain size using the relationship reported in figure 1(b). As-synthesised: the spectrum recorded on nanorods [30]; After HT (heat treatment) 600 K: spectrum recorded on the sample after thermal annealing at 600 K. Laser shot border and centre: spectra recorded on the periphery and central part of the pellet, respectively. No uncertainty bands could be associated to the melted and refrozen grain size. (c), (d) TEM images of nc-ThO_2 sample after a laser heating cycle. The insert picture in (c) is the FFT (fast Fourier transform) image of the region indicated. According to Raman analysis, picture (c) is part of the central molten zone of the sample, whereas the structure in (d) comes from the periphery of the sample.

after the laser heating experiments (figure 2(f)). The aerosol observed can be divided in two classes: spherical individual particles of a few μm diameter and smaller (size of hundreds of nm) polyhedral structures (figure 2(f)). The first kind of particles may originate from the liquid matrix, expelled by mechanical shock wave induced by the laser impact, whereas the smaller nanometric particles might be formed by rapid condensation of the vapour [49].

Direct observation of crystallites after laser heating is extremely hard by TEM (for which the 'refrozen' grains would be too large) and by PXRD (for which the mass of melted material —much less than one mg—would be too little). This fast formation of large crystallites was observed in this work with the help of micro-Raman spectroscopy. The linear relationship previously reported (figure 1(b)) was used in order to map local grain sizes in samples after the laser heating experiments, as shown in figures 3(a) and (b). It can be seen that only the central part shows a large and obvious grain size increase. The crystallite size estimation obtained using Raman spectroscopy was qualitatively in agreement with TEM analyses, which showed big crystalline domains of hundreds of nm (figure 3(c)), but also that small grains were still present

(mean size 20 nm, figure 3(d)). The smallest grains were located at the border of the pellet, whereas the bigger ones were part of the central, melted and refrozen surface.

The current experiments provide, therefore, first evidence that a very large and fast growth of the grain size, certainly resulting from a solid–liquid–solid phase transition, occurs for this nano-crystalline refractory oxide at temperatures well below (400 K to 600 K) the melting point of the corresponding bulk material.

The several phenomena observed at very high temperature (melting, vaporization, formation of aerosols and variation of optical properties) resulted in a radiance signal too complex to permit a more precise estimate of the eventual melting temperature depression. Nonetheless, the present observations ensure that big and obvious differences exist between the high temperature behaviours of bulk and nc-thorium dioxide. They constitute therefore a first important step into a challenging and intriguing research field, which can logically be extended to the analysis of other nanostructured refractory materials.

4. Conclusions

An exploratory experimental approach for the study of the very high-temperature behaviour (close to the melting transition) of nanocrystalline (around 4 nm) refractory ThO_2 was successfully applied in the present work. Very likely formation of metastable liquid from the nanostructured ThO_2 was observed between 400 K and 600 K below the melting temperature of the corresponding bulk material (3631 K), giving first proof that melting-point depression due to grain size effect can be huge also for nanostructured refractory oxides with very small grains. The local mapping after melting of the grain structure in ThO_2 samples has been done by means of Raman spectroscopy, as vibrational properties change according to grain size, mainly due to phonon confinement, in the crystalline domain. The use of this technique allowed a local analysis on the micro-scale, and avoided destruction of the sample and time-consuming sample preparation. The experimental approach adopted will therefore be used to investigate other nanostructured and Raman sensitive refractory oxides.

Acknowledgements

The authors are indebted to G Pagliosa, D Bouexière, M Ernstberger, B Cremer and T Wiss (JRC-ITU) for the sample characterization, R Böhler and P Cakir (JRC-ITU) for their help in the laser heating experiments. Special thanks are conveyed to V V Rondinella, P Raison (JRC-ITU), C E Bottani (Politecnico di Milano) and G Gouadec (Université Paris VI) for their scientific advice.

Appendix A

Phonon confinement model

A Gaussian weighting function [42, 50] was employed to fit experimental data for crystallites whose size is in the limit of the applicability of the phonon confinement model, i.e., particle diameter bigger than ≈5–10 nm [17]. As inhomogeneous strain related to grain size dispersion can also contribute to the peak broadening and shift, particle size distribution was considered, as

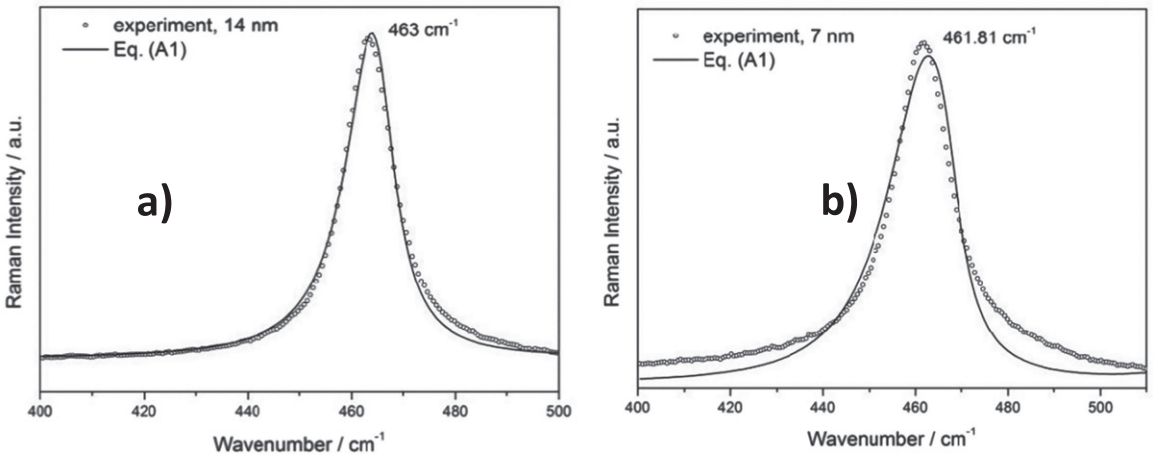

Figure A.1. (a) First-order Raman T_{2g} peak of a nc-ThO_2 sample with average crystallite size of 14 nm (open circles) and thefitted spectrum (solid line) using equation (A.1). (b) First-order Raman T_{2g} peak of a nc-ThO_2 sample with average crystallite size of 7 nm (open circles) and the fitted spectrum (solid line) using equation (A.1).

determined by TEM (see table S1 in the online supplementary data). No variation of the lattice parameter was measured for the NCs sample (see supporting information in [31]), so no microstrain effect was included in the model. According to the model, the Raman intensity $I(\omega)$ of the triply degenerate T_{2g} mode was calculated over the whole Brillouin zone (BZ), assumed to be spherical and isotropic, by the following relation [22]:

$$I(\omega) \propto \sum_{1}^{3} \int_{0}^{\infty} \rho(D)\, dD \times \int_{BZ} \frac{\exp\left(-q^2 D^2/2\beta\right)}{\left[\omega - \omega_i(q)\right] + \left[\Gamma_0/2\right]^2} d^3q \qquad \text{(A.1)}$$

where $\rho(D)$ is the particle size distribution, D the particle size, the reduced wave vector, Γ_0 is the linewidth of the Raman mode in the bulk crystal, $\omega_i(q)$ the ith branch of the phonon dispersion curve of the T_{2g} mode, here assumed to be $\omega_i(q) = \omega_0 - \Delta\omega_i \sin^2\left(\frac{qa}{2}\right)$ [19], where $\Delta\omega_i$ are calculated from the curves reported in [40] and ω_0 is the measured wavenumber of the T_{2g} mode in bulk material, β the confinement factor. The calculated Raman spectra (solid line) for 14 nm size ThO_2 and the experimental data (dotted line) are presented in figure A.1(a). In the calculated spectrum the value of the confinement factor β was set as parameter. The best fit was obtained for $\beta = 7.919$ considering opportune scaling of the contribution of the three branches. It was not always possible to obtain good agreement between the different experimental spectra and the calculated ones using this parameter value, probably due to limited applicability of the model when the particle size gets smaller (see figure A.1(b)).

References

[1] Roduner E 2006 Introduction *Nanoscopic Materials: Size-Dependent Phenomena* (Cambridge: Royal Society of Chemistry) pp 1–3
[2] Lohse S E and Murphy C J 2012 *J. Am. Chem. Soc.* **134** 15607–20
[3] Goesmann H and Feldmann C 2010 *Angew. Chem. Int. Ed.* **49** 1362–95

[4] Alivisatos A P 1997 *Endeavour* **21** 56–60
[5] Somorjai G A, Tao F and Park J Y 2008 *Top. Catal.* **47** 1–14
[6] Lohse S E and Murphy C J 2013 *Chem. Mater.* **25** 1250–61
[7] Thomson W 1871 *Phil. Mag.* **42** 448–52
[8] Pawlow P 1909 *Z. Phys. Chem.* **65** 1–35
[9] Buffat P and Borel J-P 1976 *Phys. Rev.* A **13** 2287–96
[10] Goldstein A N, Echer C M and Alivisatos A P 1992 *Science* **256** 1425–7
[11] Lai S L, Guo J Y, Petrova V, Ramanath G and Allen L H 1996 *Phys. Rev. Lett.* **77** 99–102
[12] Lai S L, Carlsson J R A and Allen L H 1998 *Appl. Phys. Lett.* **72** 1098–100
[13] Castro T, Reifenberger R, Choi E and Andres R P 1990 *Phys. Rev.* B **42** 8548–56
[14] Takagi M J 1954 *J. Phys. Soc. Japan* **9** 359–63
[15] Coombes C J 1972 *J. Phys. F: Met. Phys.* **2** 441–9
[16] Manara D, Sheindlin M, Heinz W and Ronchi C 2008 *Rev. Sci. Instrum* **79** 113–9
[17] Gouadec G and Colomban P 2007 *Prog. Cryst. Growth Ch.* **53** 1–56
[18] Diéguez A, Romano-Rodriguez A, Morante J R, Bârsan N, Weimar U and Gögel W 1997 *Appl. Phys. Lett.* **71** 1957–9
[19] Arora A K, Rajalakshmi M, Ravindran T R and Sivasubramanian V 2007 *J. Raman Spectrosc.* **38** 604–17
[20] Spanier J E, Robinson R D, Zhang F, Chan S-W and Herman I P 2001 *Phys. Rev.* B **64** 2454071–8
[21] Rajalakshmi M, Akora A K, Bendre B S and Mahamuni S 2000 *J. Appl. Phys.* **87** 2445–8
[22] Popović Z V, Dohčević Z, Konstantinović M J and Šćepanović M 2007 *J. Raman Spectrosc.* **38** 750–5
[23] Li Bassi A, Cattaneo D, Russo V, Barborini E, Mazza T, Piseri P, Milani P, Ernst F O, Wegner K, Pratsinis S E and Bottani C E 2005 *J. Appl. Phys.* **98** 0743051–9
[24] Zhu K-R, Zhang M-S, Chen Q and Yin Z 2005 *Phys. Lett.* A **340** 220–7
[25] Yashima M, Hoshina T, Ishimura D, Kobayashi S, Nakamura W, Tsurumi T and Wada S 2005 *J. Appl. Phys.* **98** 0143131–8
[26] Kosacki I, Suzuki T, Anderson H U and Colomban P 2002 *Solid State Ionics* **149** 99–105
[27] Ronchi C and Hiernaut J P 1996 *J. Alloys Comp.* **240** 179–85
[28] Benz R 1969 *J. Nucl. Mater.* **29** 43–9
[29] Keramidas V G and White W B 1973 *J. Chem. Phys.* **59** 1561–2
[30] Hudry D, Apostolidis C, Walter O, Gouder T, Courtois E, Kübel C and Meyer D 2012 *Chem. Eur. J.* **18** 8283–7
[31] Hudry D, Apostolidis C, Walter O, Gouder T, Courtois E, Kübel C and Meyer D 2013 *Chem. Eur. J.* **19** 5297–305
[32] Shi W-Q, Yuan L-Y, Li Z-J, Lan J-H, Zhao Y-L and Chai Z-F 2012 *Radiochim. Acta* **100** 727–36
[33] Spino J, Santa Cruz H, Jovani-Abril R, Birtcher R and Ferrero C 2012 *J. Nucl. Mater.* **422** 27–44
[34] Manara D, Ronchi C, Sheindlin M, Lewis M and Brykin M 2005 *J. Nucl. Mater.* **342** 148–63
[35] De Bruycker F, Boboridis K, Manara D, Poeml P, Rini M and Konings R J M 2010 *Materials Today* **13** 52–5
[36] Böhler R, Welland M J, De Bruycker F, Boboridis K, Janssen A, Eloirdi R, Konings R J M and Manara D 2012 *J. Appl. Phys.* **111** 113501–8
[37] Manara D, Böhler R, Boboridis K, Capriotti L, Quaini A, Luzzi L, De Bruycker, Guéneau C, Dupin N and Konings R J M 2012 *Proc. Chem.* **7** 505–12
[38] Rajalakshmi M, Arora A K, Dash S and Tyagi A K 2003 *J. Nanosci. Nanotech.* **3** 420–2
[39] Dash S, Singh A, Ajikumar P K, Subramanian H, Rajalakshmi M, Tyagi A K, Arora A K, Narasimhan S V and Raj B 2002 *J. Nucl. Mater.* **303** 156–68
[40] Ishigame M and Kojima M 1976 *J. Phys. Soc. Japan* **41** 202–10
[41] Nemanich R J and Solin S A 1979 *Phys. Rev.* B **20** 392–401
[42] Richter H, Wang Z P and Ley L 1981 *Solid State Commun.* **39** 625–9
[43] Martynenko Y V and Ognev L I 2005 *Tech. Phys.* **50** 130–2
[44] Wang C X and Yang G W 2005 *Mat. Sci. Eng.* R **49** 157–202

[45] Berry R S 1999 Phases and phase changes of small systems *Theory of Atomic and Molecular Clusters. With a Glimpse at Experiments* ed J Jellinek (Berlin: Springer) pp 1–26
[46] Hill T L and Chamberlin R V 1998 *Proc. Natl. Acad. Sci. USA* **95** 12779–82
[47] Biloni H and Boettinger W J 1996 Solidification *Physical Metallurgy* vol 1(4th revised and enhanced edition) ed R W Cahn and P Haasen (Amsterdam: Elsevier) pp 669–842
[48] Kingery W D, Bowen H K and Uhlmann D R 1976 *Introduction to Ceramics* 2nd edn (New York: Wiley)
[49] Di Lemma F G, Colle J Y, Ernstberger M, Rasmussen G, Thiele H and Konings R J M 2014 *J. Aerosol Science* **70** 36–49
[50] Campbell I H and Fauchet P M 1986 *Solid State Commun.* **58** 739–41